



**Voltage gated inter-cation selective ion channels from
graphene nanopores**

Journal:	<i>Nanoscale</i>
Manuscript ID	NR-COM-12-2018-010360.R1
Article Type:	Communication
Date Submitted by the Author:	25-Apr-2019
Complete List of Authors:	<p>Cantley, Lauren; Boston University, Swett, Jacob; Lockheed Martin Space Systems Lloyd, David; Boston University Cullen, David; Oak Ridge National Laboratory, Materials Science & Technology Division ZHOU, KE; Tsinghua University Bedworth, Peter; Lockheed Martin Space Systems Heise, Scott; Lockheed Martin Space Systems Rodinone, Adam; Oak Ridge National Laboratory Xu, Zhiping; Tsinghua University, Engineering Mechanics Sinton, Steve; Lockheed Martin Space Systems Bunch, Scott; Boston University, Mechanical Engineering</p>



Voltage gated inter-cation selective ion channels from graphene nanopores

Received 00th January 20xx,
Accepted 00th January 20xx

Lauren Cantley^a, Jacob L. Swett^b, David Lloyd^a, David A. Cullen^c, Ke Zhou^d, Peter V. Bedworth^b, Scott Heise^b, Adam J. Rondinone^e, Zhiping Xu^d, Steve Sinton^b, J. Scott Bunch^{a,f,*}

DOI: 10.1039/x0xx00000x

www.rsc.org/

With the ability to selectively control ionic flux, biological protein ion channels perform a fundamental role in many physiological processes. For practical applications that require the functionality of a biological ion channel, graphene provides a promising solid-state alternative, due to its atomic thinness and mechanical strength. Here, we demonstrate that nanopores introduced into graphene membranes, as large as 50 nm in diameter, exhibit inter-cation selectivity with a ~20x preference for K⁺ over divalent cations and can be modulated by an applied gate voltage. Liquid atomic force microscopy of the graphene devices reveals surface nanobubbles near the pore to be responsible for the observed selective behavior. Molecular dynamics simulations indicate that translocation of ions across the pore likely occurs via a thin water layer at the edge of the pore and the nanobubble. Our results demonstrate a significant improvement in the inter-cation selectivity displayed by a solid-state nanopore device and by utilizing the pores in a de-wetted state, offers an approach to fabricating selective graphene membranes that does not rely on the fabrication of sub-nm pores.

The main text of the article Protein ion channels, which are vital for many biological processes, including cell signaling and volume regulation within cells, are remarkably effective due to their high selectivity, permeability, and gating¹. This has motivated the development of solid-state devices that mimic their function for practical applications in sensing, separation, therapeutics, and neuromorphic computing. Solid-state nanochannel and nanopore transistors have previously been used to manipulate ionic transport²⁻

³; however, thus far they have been limited by low electrolyte concentrations⁴⁻⁵, high applied voltages^{3,6}, or a combination of the two⁷.

Graphene nanopores have been explored for applications in sensing and separations, and are a promising material for a solid-state ion channel. Aside from graphene being atomically thin⁸, mechanically strong⁹, and relatively inert¹⁰, it has been shown that well-defined nanometer and sub-nanometer pores can be controllably introduced into the material¹¹⁻¹⁷. Nanopores in graphene have been shown to exhibit ion selectivity^{12, 18-24} and gated nanopores in graphene have been used in sensing biomolecules such as DNA and proteins²⁵⁻²⁶. However, graphene nanopores have yet to mimic the degree of inter-cation selectivity exhibited by protein ion channels.

For the nanopore devices studied here, single-layer graphene was obtained by CVD growth. Suspended graphene membranes were fabricated by transferring graphene over an approximately 5 μm diameter hole etched in a suspended silicon nitride window coated with 20 nm of atomic-layer-deposited (ALD) alumina. A gold electrode was patterned in contact with the suspended graphene membrane via a shadow mask. Suspended graphene devices were mounted in a custom-made microfluidic cell, allowing for the introduction of electrolyte solution to both sides of the graphene membrane. Measurement of conductance across the graphene membrane was carried out by applying a bias voltage across the device and measuring the resulting current (Fig. 1a). The microfluidic cell allowed for electrical contact to the gold electrode, permitting the application of a gate voltage to the graphene while sweeping the transmembrane bias voltage. Additionally, the microfluidic cell was designed to allow atomic force microscopy (AFM) access to the top side of the membrane such that the pore could be imaged while in solution. Devices made from unperforated graphene had a transmembrane conductance below 150 pS in 0.1 M KCl and 280 pS in 1 M KCl, confirming that graphene is a good barrier to ionic conductance. Graphene devices were perforated via helium ion microscope (HIM) drilling. Scanning transmission electron microscopy (STEM), HIM, and AFM were used to measure the pore diameters and observe the pore structure (Fig. 1b, 1c).

Ionic conductance was first measured in a two-terminal configuration across each device, with the gate terminal floating. For

^a Address here.

^b Department of Mechanical Engineering, Boston University, Boston, Massachusetts 02215, USA.

^c Advanced Technology Center, Lockheed Martin Space, Palo Alto, California, 94304, USA.

^d Materials Science and Technology Division, Oak Ridge National Laboratory, Oak Ridge, Tennessee, 37831, USA.

^e Applied Mechanics Laboratory, Department of Engineering Mechanics and Center for Nano and Micro Mechanics, Tsinghua University, Beijing 100084, China.

^f Center for Nanophase Materials Sciences, Oak Ridge National Laboratory, Oak Ridge, Tennessee, 37831, USA.

^g Division of Materials Science and Engineering, Boston University, Brookline, Massachusetts 02446, USA.

Electronic Supplementary Information (ESI) available: [details of any supplementary information available should be included here]. See DOI: 10.1039/x0xx00000x

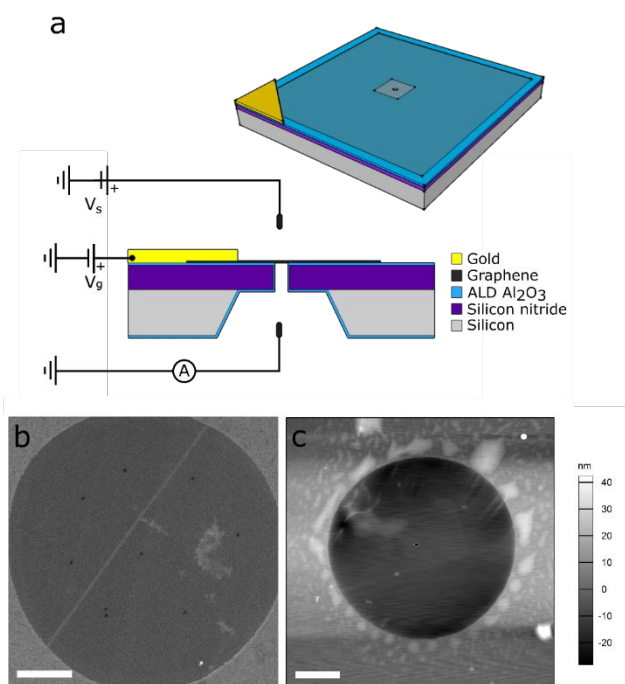


Figure 1. Experimental set up. (a) 3D rendering of the device along with schematic of the measurement circuit and cross section of the device. Graphene is suspended over a 5 μm hole in the silicon nitride window and mounted in a custom microfluidic cell in which electrolyte solution is introduced to both sides of the graphene membrane. (b) HIM image of CVD graphene with nine 35 nm pores drilled using HIM. (c) AFM image in air of CVD graphene with a single 50 nm pore drilled using HIM. Scale bars = 1 μm .

the graphene device in figure 1b, non-linear (activated) I-V characteristics were observed using monovalent electrolyte solutions (Fig. 2a). To account for the differences in bulk conductivity, the normalized conductance was plotted for each cation-chloride solution

$$g_i = \frac{G_i}{\sigma_i / \sigma_{KCl}} \quad (1)$$

where G_i is the measured nanopore conductance in solution i , σ_i is the bulk conductivity of solution i and σ_{KCl} is the bulk conductivity of KCl at a comparable chloride concentration. The normalized conductance reveals the pore(s) to be highly cation selective, with significant preference for K^+ over other ions measured. For the device shown in figure 1b at $V_g = 0$ mV, the normalized conductance of KCl was $\sim 4\times$ greater than the other monovalent ions (Na^+ and Li^+) and $\sim 20\times$ greater than the divalent ion measured (Ca^{2+}) (Fig. 2b). The differences in normalized conductance as well as the absence of conductivity in CaCl_2 suggest that the dominant charge carriers are cations; additional experiments using asymmetric ion conditions confirm this result (SI Appendix, Fig. S2).

Next, a gate voltage was applied to the graphene to modulate the ionic current. Before proceeding with voltage-gated measurements, leakage current from source/drain to gate was measured to be less than 300 pA at 500 mV, verifying the device conductance was governed by ion transport and not a result of leakage current. The pore current was then measured under various applied gate voltages. Figure 2c demonstrates the ionic current response to changes in the gate voltage. As a more negative gate voltage is applied, the ionic current increased. As positive gate

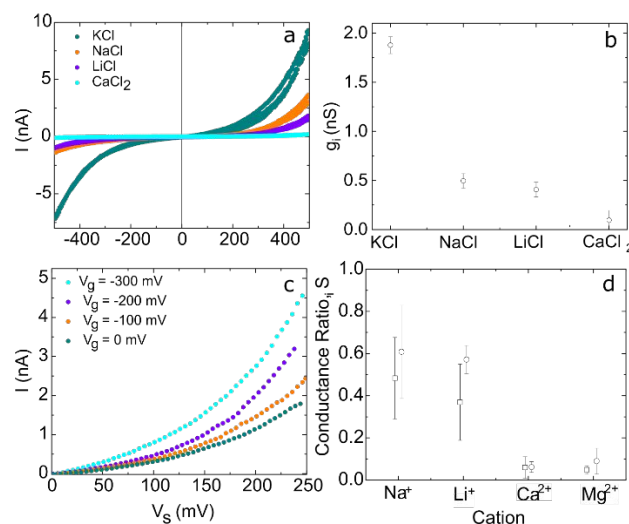


Figure 2. Current-voltage characteristics. (a) I-V curves and (c) gating behavior for the device in figure 1b. (b) Conductance taken at $V_s = 0$ mV for various electrolyte solutions. X-axis is ordered from lowest to highest cation hydration energy. All solutions are at 0.1 M chloride concentrations. (d) Inter-cation conductance ratio (S_i) of graphene nanopores sorted by cation. Open squares and open circles represent mean and standard deviation for devices with nine ~ 30 nm pores (for S_{Na} : $N=5$, S_{Li} , S_{Ca} : $N=4$, S_{Mg} : $N=3$) and devices with a single ~ 50 nm pore (S_{Na} , S_{Li} , S_{Mg} : $N=3$, S_{Ca} : $N=2$), respectively.

voltage was applied, there was no significant change in the ionic conductivity. This unipolar behavior is similar to a p-type FET device, likewise suggesting that cations are the majority charge carriers, and is consistent with 2 terminal measurements²⁷⁻²⁹.

To characterize the selectivity of a device, we define the conductance ratio as $S_i = g_i / g_{KCl}$. This definition gives a conductance ratio of 1 for a pore that does not distinguish between cation i and K^+ . The conductance ratio was measured for 10 graphene devices with HIM drilled pores. Six devices had nine approximately 30 nm diameter pores, the same configuration as the device shown in figure 1b, and four had a single 50 nm diameter pore, shown in figure 1c. Five of the six nine-pore devices and three of the four single pore devices displayed selective behavior. The mean conductance ratio for these devices is plotted in figure 2d. All samples displayed a similar trend in selectivity, where divalent ions had a lower conductance ratio than the monovalent species measured.

The activated IV behavior and observed selectivity in figure 2 inversely scales with the trend in hydrated radii of the measured cations, $\text{K}^+ < \text{Na}^+ < \text{Li}^+ < \text{Ca}^{2+} < \text{Mg}^{2+}$ ^{1, 23}, where K^+ has the highest conductance. Additionally, the ability to detect an electrostatic gating response in solution is dependent on the Debye screening length: a measure of a charge carrier's electrostatic range in solution (~ 1 nm and ~ 0.3 nm in 0.1 M and 1M KCl, respectively). The pore diameter of a fully wet pore should be within a given solution's Debye length in order to observe direct electrostatic gating effects. However, the discrepancy between imaged pore size and the observed selective gate-responsive behavior suggests that the pores are not fully wet. Similarly, the absolute value of the conductance across the graphene pore is lower than one would expect given a standard model for pore conductance based on the imaged pore diameter³⁰; this also suggests incomplete wetting.

Incomplete wetting of a pore occurs often in nanopore experiments, particularly on hydrophobic surfaces³¹. Nanoscale surface bubbles are known to be present and highly stable on hydrophobic surfaces, such as highly oriented

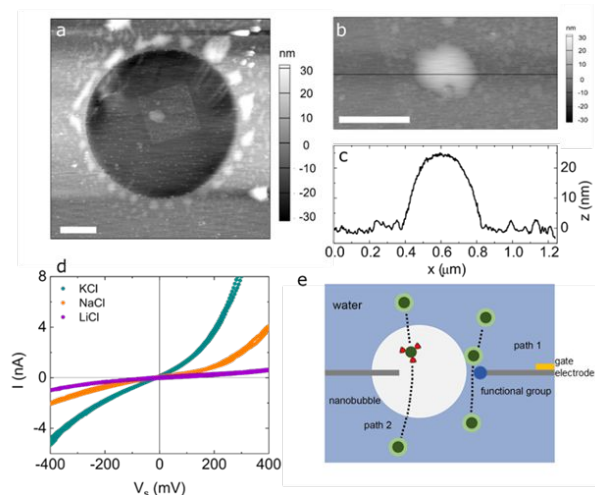


Figure 3. Liquid AFM imaging. (a) AFM image of a graphene membrane in water reveals bubbles on the surface of the graphene (compare to Fig. 1c of the same device measured in air). The square outline surrounding the large bubble corresponds with the area of graphene exposed during HIM drilling, which likely modified the surface of the graphene. Scale bar = 1 μm . (b) High magnification AFM image of bubble over pore (scale bar = 500 nm) and (c) corresponding cross sectional line cut. (d) Conductance measurements across device shown in (a) demonstrate non-linear, selective I-V behavior. (e) Schematic illustration of the two transport pathways considered during MD simulations. Gray planes represent the graphene and the dark blue circle on the edge is functional group. The dark green circles are ions and the outer light green parts are hydration water. The inner white region indicates the bubble. In path 1, the ion travels along the edge of the graphene nanopore, whereas in path 2, ions are transported through the water/gas interface.

pyrolytic graphite, and occur in at least three types: gaseous nanobubbles, nanobubbles composed of oil⁴⁵, and solid nanoparticles⁴⁶. They are often produced via the exchange of ethanol to aqueous solution, a procedure utilized in the wetting of our graphene devices³². STEM imaging of our devices reveals a concentration of hydrocarbons adsorbed onto the surface of the graphene near the pore (SI Appendix, Fig.S3). The presence of these surface adsorbates not only modifies the wettability and the surface charge of the pore, but provide favorable locations (such as step edges or defects) for a nanobubble to pin³³. AFM imaging of a graphene device in water revealed a nanobubble on the surface of the graphene, occluding the pore (Figure 3a-c, SI Appendix, Fig.S4-S6). Subsequent conductance measurements across the device show selective activated I-V behavior similar to that observed in previous devices (Figure 3d, Figure 2). While the presence of nanobubbles was found to be ubiquitous, our limited control over the bubble formation may explain the variability in figure 2d. Within the devices studied, selective behavior was observed with the presence of a nanobubble occluding all or part of the pore area. Conversely, the device AFM imaged in water that did not possess a nanobubble displayed linear, non-selective I-V characteristics with a conductance consistent with the theoretically expected value for the imaged pore size (SI Appendix, Fig.S7-S8).

To better understand the ion translocation process across a nanobubble at the entrance of a graphene nanopore, we performed molecular dynamics (MD) simulations to explore the free energy profiles (SI Appendix, Fig.S1). Considering the limitation of computational cost, we simulated water-immersed porous graphene membranes containing nanopores with radii in the range of 0.9-2.0 nm, with graphene edges functionalized by carbonyl groups and a gaseous nanobubble partially occluding the pore. As illustrated in Figure 3e, two transport

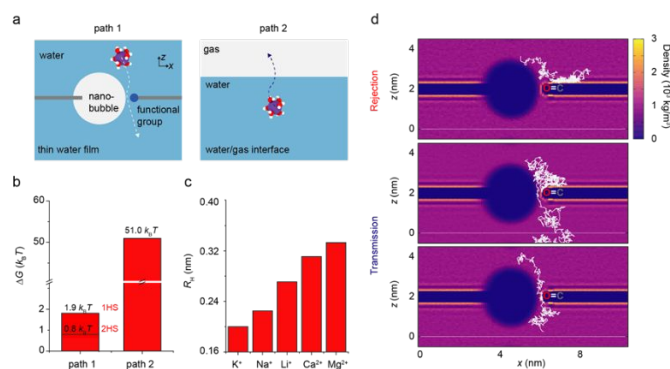


Figure 4. MD simulations. (a) Illustration of molecular simulation models and transport pathways (annotated by the dash arrows). Along path 1, ions travel along the edge of graphene nanopore coated by a thin water film, experiencing a free energy barrier of a few $k_B T$. Along path 2, ions are transported through the water/gas interface, experiencing a remarkably high free energy barrier of 51 $k_B T$. (b) Free energy barriers calculated for path 1 and 2, where 1HS/2HS indicate the situation where the 1st/2nd HS is perturbed by the functionalized graphene edge. (c) Hydration radii of ions for ions confined in nanometer-thick water films. (d) Ion diffusion under an external electric field. The ions can be translocated or rejected, demonstrating the gating effect through a thin water layer coating graphene edges, which can be controlled by the strength of external electric field. Color indicates the density of water. The trajectories are extracted from the simulation results when the strength of the electric field is 0.1 V/nm applied in the z direction. From top to bottom, $E_y = 0.01$ eV/nm, 0.1 eV/nm, and 1.00 eV/nm, respectively.

pathways were considered for the ion translocation. In path 1, ions travel through a thin 1 nm thickness water film coating the graphene edges, where the hydration shells (HSs) can be perturbed by the (functionalized) graphene edges. Here the water film thickness is defined as the distance between the water surface and the edge carbon atoms in graphene. In path 2, the HSs must be stripped off, for the ion to translocate across the water/gas interface.

We calculate the potential of mean force (PMF) from the MD simulation, to measure the change of free energy during the ion translocation process (Figure 4). For path 2, across the water/gas interface, a simple but over-estimation of the free energy barrier is $\Delta G = (1 - 1/\epsilon)q^2/(4\pi\epsilon_0 R) \approx 10$ eV by using the Born model with the assumption that the HSs are fully detached from the ions⁴¹. Here $\epsilon \approx 80$ is the relative permittivity of water and ϵ_0 is the vacuum permittivity. Our MD simulations show, however, that the HSs are partially retained as the ion translocates across the interface. The free energy barrier is reduced to 51.0 $k_B T$ as a result, which is still very significant compared to the thermal fluctuation, indicating that the hydrated ion prefers to stay in the solvent and transport along path 2 is prohibited (Figure 4a).

Conversely, the free energy barrier along path 1, through the thin water layer of 1 nm coating the graphene edge, is much reduced. Our free energy analysis shows that with the HSs perturbed, or ions captured by the functional groups at the graphene edge⁴², the barriers for the adsorption-desorption process are on the order of $k_B T$. Specifically, the barrier for Na^+ with a perturbed 2nd or 1st HS is $\Delta G = 0.8$ or 1.9 $k_B T$ (Figure 4b), respectively, which is accessible via thermal diffusion and can be enhanced by the applied electrical field.

To explain the contrast between the conductivity of ions, we calculated the hydration radii R_H of the ions and conclude with the order $\text{K}^+ < \text{Na}^+ < \text{Li}^+ < \text{Ca}^{2+} < \text{Mg}^{2+}$ (Figure 4c), which indicates that ion translocation measured in our experiments is manifested in a size-sieving mechanism. This aligns with the fact that the thickness of

water layer is comparable with R_H plus the van der Waals distances. These results also suggest that one could further engineer the functional groups of graphene edges to gain control of the selectivity³⁴.

The existence of a finite free energy barrier ΔG on the order of $k_B T$ indicates a prominent gating effect on the ion translocation process. To explore the gating effect, we carry out non-equilibrium MD simulations by applying an external field $E_y = 0.01$ -1.00 eV/nm, and counting the probability of transmission and rejection events (Figure 4d). The results suggest that the transmission probability of ions through the water film measured in a fixed time interval increases with the field strength, demonstrating less torturous trajectories.

Conclusions

In summary, graphene nanopore devices occluded by a surface nanobubble demonstrated strong inter-cation selectivity, and ionic transport was modulated by an applied gate voltage. By utilizing pores in a de-wetted state, we have demonstrated a cation selective solid-state nanopore device that does not rely on the controlled fabrication of sub-nm pores. MD simulation results indicate that the ion selectivity can be explained by ion transport occurring across thin water films along the edge of the graphene pore, with transmission across the pore highly dependent on an externally applied electric field. Development of a defined process for control of nanobubbles will be necessary for further enhancing selectivity control. This ability to control selective nanopores at low voltages (< 500 mV) and with biologically relevant concentrations (100 mM) is an exciting advancement in sensing and separation technologies, not only providing a solid-state analog to voltage-gated biological ion channels, but having potential for applications in nanofluidic circuitry, water filtration, and energy storage as well.

Conflicts of interest

There are no conflicts to declare.

Author Contributions

L.C. and D.L. performed the experiments. L.C., J.L.S. and J.S.B. conceived and designed the experiments. L.C., J.L.S., S.H., P.V.B., D.L. prepared and fabricated the samples. J.L.S., D.A.C., and A.J.R. performed HIM and STEM perforation and imaging. D.L. performed AFM imaging. K.Z. and Z.X. carried out molecular dynamics simulations. L.C., J.L.S., D.L., D.A.C., A.J.R., P.V.B., K.Z., Z.X., S.S. and J.S.B. interpreted the results and co-wrote the manuscript.

Acknowledgements

The authors acknowledge K. Ekinici for the use of the optical table, C. Duan for lab use and useful discussions. This work was funded by the National Science Foundation (NSF), grant no. 1054406 (CMMI: CAREER, Atomic Scale Defect Engineering in Graphene Membranes), grant no. 1706322 (CBET: Bioengineering of Channelrhodopsins for Neurophotonic and Nanophotonic Applications) and by the NSF Graduate Research Fellowship Program under grant no. DGE-1247312. HIM perforation and aberration-corrected STEM imaging

were conducted at Oak Ridge National Laboratory's Center for Nanophase Materials Sciences (CNMS), a U.S. Department of Energy Office of Science User Facility.

Notes and references

- Hille B (2001) *Ion Channels of Excitable Membranes*. (Sinauer Associates Inc, Sunderland, MA, Ed. 3), pp 329.
- Siwy Z, Howorka S (2010) Engineered voltage-responsive nanopores. *Chem Soc. Rev.* **39**:115-1132.
- Guan W, Li S X, Reed M A (2014) Voltage gated ion and molecule transport in engineered nanochannels: theory, fabrication and applications. *Nanotechnology* **25**:122001.
- Fan R, Huh S, Yan R, Arnold J, Yang P (2008) Gated proton transport in aligned mesoporous silica films. *Nat. Mater.* **7**:303-307.
- Nam S W, Rooks M J, Kim KB, Rosnagel S M (2009) Ionic field effect transistors with sub-10 nm multiple nanopores. *Nano Lett.* **9**:2044-2048.
- Karnik R, Fan R, Yue M, Li D, Yang P, Majumdar A (2005) Electrostatic control of ions and molecules in nanofluidic transistors. *Nano Lett.* **5**:943-948.
- Lee SH, Lee H, Jin T, Park S, Yoon BJ, Sung GY, Kim KB, Kim SJ (2015) Sub-10nm transparent all-around-gated ambipolar ionic field effect transistor. *Nanoscale*. **7**:936-946.
- Meyer J C, Geim A K, Katsnelson M I, Novoselov K S, Booth T J, Roth S (2007) The structure of suspended graphene sheets. *Nature* **446**:60-63.
- Lee C, Wei X, Kysar J W, Hone J (2008) Measurement of the elastic properties and intrinsic strength of monolayer graphene. *Science* **321**:385-388.
- Chen S, Brown L, Levendorf M, Cai W, Ju SY, Edgeworth J, Li X, Magnuson C W, Velamakanni A, Piner R D, Kang J, Park J, Ruoff R S (2011) Oxidation resistance of graphene-coated Cu and Cu/Ni alloy. *ACS Nano* **5**:1321-1327.
- Liu L, Ryu S, Tomasik M R, Stolyarova E, Jung N, Hybertsen M S, Steigerwald M L, Brus L E, Flynn G W (2008) Graphene oxidation: thickness-dependent etching and strong chemical doping. *Nano Lett.* **8**:1965-1970.
- O'Hern S C, Boutilier M S H, Idrobo, JC, Song Y, Kong J, Laoui T, Atieh M, Karnik R (2014) Selective ionic transport through tunable subnanometer pores in single-layer graphene membranes. *Nano Lett.* **14**:1234-1241.
- Surwade S P, Smirnov S N, Vlasiouk I V, Unocic R R, Veith G M, Dai S, Mahurin S M (2015) Water desalination using nanoporous single-layer graphene. *Nat. Nanotech.* **10**:459-464.
- Kidambi P R, Nguyen G D, Zhang S, Chen, Q, Kong J, Warner J, Li AP, Karnik R (2018) Facile Fabrication of Large-Area Atomically Thin Membranes by direct Synthesis of Graphene with Nanoscale Porosity. *Advanced Materials* **0**(0):1804977.
- Lee D H, Kim J E, Han T H, Hwang J W, Jeon S, Choi S-Y, Hong S H, Lee W J, Ruoff R S, Kim S O (2010) Versatile carbon hybrid films composed of vertical carbon nanotubes grown on mechanically compliant graphene films. *Adv. Mat.* **22**:1247-1252.
- Yun J M, Kim K N, Kim J Y, Shin D O, Lee W J, Lee S H, Lieberman M, Kim S O (2011) DNA origami nanopatterning on chemically modified graphene. *Angew. Chem.* **124**: 936-939
- Maiti U N, Thapa R, Lim J, Li D J, Kim K H, Kim S O (2015) Self-size-limiting nanoscale perforation of graphene for heteroatom doping. *ACS Appl. Mater. Interfaces* **7**(46):25898-25905.

18. Koenig S P, Wang L, Pellegrino J, Bunch J S (2012) Selective molecular sieving through porous graphene. *Nat. Nanotech.* **7**:728-732.
19. O'Hern S C, Jang D, Bose S, Idrobo JC, Song Y, Laoui T, Kong J, Karnik R (2015) Nanofiltration across defect-sealed nanoporous monolayer graphene. *Nano Lett.* **15**:3254-3260.
20. Jian T, Rasera BC, Guerrero RJ, Boutilier MS, O'Hern SC, Idrobo JC, Karnik R (2015) Heterogeneous sub-continuum ionic transport in statistically isolated graphene nanopores. *Nat. Nanotech.* **10**:1053-1057.
21. Rollings R C, Kuan A T, Golovchenko J A (2016) Ion selectivity of graphene nanopores. *Nature Comm.* **7**:11408.
22. Walker M I, Ubych K, Saraswat V, Chalklen E A, Braeuninger-Weimer P, Caneva S, Weatherup R S, Hofmann S, Keyser U F (2017) Extrinsic Cation Selectivity of 2D Membranes. *ACS Nano.* **11**:1340-1346.
23. Sint K, Wang B, Král P (2008) Selective ion passage through functionalized graphene Nanopores. *J. Am. Chem. Soc.* **130**:16448-16449.
24. Li S, Lee JH, Hu Q, Oh TS, Yoo JB (2018) Scalable graphene composite membranes for enhanced ion selectivity. *Journal of Membrane Science.* **564**:159-165.
25. Venkatesan B M, Estrada D, Banerjee S, Jin X, Dorgan V E, Bae MH, Aluru N R, Pop E, Bashir R (2012) Stacked graphene-Al₂O₃ nanopore sensors for sensitive detection of DNA and DNA-protein complexes. *ACS Nano.* **6**:441-450.
26. Traversi F, Raillon C, Benameur S M, Liu K, Khlybov S, Tosun M, Krasnozhan D, Kis A, Radenovic A (2013) Detecting the translocation of DNA through a nanopore using graphene nanoribbons. *Nat. Nanotech.* **8**:939-945.
27. Fan R, Huh S, Yan R, Arnold J, Yang P (2008) Gated proton transport in aligned mesoporous silica films. *Nat. Mater.* **7**:303-307.
28. Nam SW, Rooks M J, Kim KB, Rossnagel S M (2009) Ionic field effect transistors with sub-10 nm multiple nanopores. *Nano Lett.* **9**:2044-2048.
29. Karnik R, Fan R, Yue M, Li D, Yang P, Majumdar A (2005) Electrostatic control of ions and molecules in nanofluidic transistors. *Nano Lett.* **5**:943-948.
30. Garaj S, Hubbard W, Reina A, Kong J, Branton D, Golovchenko J A (2010) Graphene as a subnanometre trans-electrode membrane. *Nature* **467**:190-193.
31. Smeets RMM, Keyser U F, Wu M Y, Dekker N H, Dekker C (2006) Nanobubbles in solid-state nanopores. *Phys. Rev. Lett.* **97**:088101.
32. Lohse D (2015) Surface nanobubbles and nanodroplets. *Rev. Mod. Phys.* **87**:981-1035.
33. Kozbial A, Li Z, Conaway C, McGinley R, Dhingra S, Vahdat V, Zhou F, D'Urso B, Liu H, Li L (2014) Study on surface energy of graphene by contact angle measurements. *Langmuir* **30**:8598-8606.
34. Song Z, Xu Z (2015) Ultimate Osmosis Engineered by the Pore Geometry and Functionalization of Carbon Nanostructures. *Scientific Reports*, **5**:10597.
35. Plimpton S (1995) Fast Parallel Algorithms for Short-Range Molecular Dynamics. *J. Comput. Phys.* **117**(1):1-19.
36. Wei N, Lv C, Xu Z (2014) Wetting of Graphene Oxide: A Molecular Dynamics Study. *Langmuir* **30**(12):3572-3578.
37. Jorgensen W L, Maxwell D S, Tirado-Rives J (1996) Development and Testing of the OPLS All-Atom Force Field on Conformational Energetics and Properties of Organic Liquids. *J. Am. Chem. Soc.* **118**(45):11225-11236.
38. Berendsen H, Grigera J, Straatsma T (1987) The Missing Term in Effective Pair Potentials. *J. Phys. Chem.* **91**(24):6269-6271.
39. Gao W (2015) The Chemistry of Graphene Oxide. *Graphene Oxide* (Springer), pp 61-95.
40. Li P, Song L F, Merz K M Jr (2015) Systematic Parameterization of Monovalent Ions Employing the Nonbonded Model. *J. Chem. Theory Comput.* **11**(4):1645-1657.
41. Weeks J D, Chandler D, Andersen H C (1971) Role of Repulsive Forces in Determining the Equilibrium Structure of Simple Liquids. *J. Chem. Phys.* **54**(12):5237-5247.
42. Roux B (1995) The Calculation of the Potential of Mean Force Using Computer Simulations. *Comput. Phys. Commun.* **91**(1-3):275-282.
43. Grossfield A (Accessed 2018) Wham: The Weighted Histogram Analysis Method. Version 2.0.6 <http://membrane.urmc.rochester.edu/content/wham>.
44. Zhou K, Xu Z (2018) Renormalization of Ionic Solvation Shells in Nanochannels. *ACS Appl. Mater. Interfaces* **10**(33):27801-27809.
45. Lohse D, Zhang X (2015) Surface nanobubbles and nanodroplets. *Rev. Mod. Phys.* **87**:981-1035.
46. Alheshibri M, Craig V SJ (2018) Differentiating between Nanoparticles and Nanobubbles by Evaluation of the Compressibility and Density of Nanoparticles. *The Journal of Physical Chemistry C* **122**(38):21998-22007.
47. An H, Tan BH, Ohl C-L (2016) Distinguishing Nanobubbles from Nanodroplets with AFM: The Influence of Vertical and Lateral Imaging Forces *Langmuir* **32**(48):12710-12715

